

# Sensing multiple scattering via multiple quantum coherence signals

Benedikt Ames, Edoardo G. Carnio, Vyacheslav Shatokhin, and Andreas Buchleitner  
*Physikalisches Institut, Albert-Ludwigs-Universität Freiburg,  
 Hermann-Herder-Str. 3, D-79104 Freiburg, Germany*  
 (Dated: June 29, 2022)

We show that multiple quantum coherence signals in dilute gases require the multiple scattering of *real* photons. The latter mediate the retarded dipole-dipole interaction – which dominates the static interatomic potential hitherto considered as the essential source of these signals.

*Introduction.*— Dipole-dipole interactions are the key mechanism behind transport and collective phenomena, including dipole blockade in Rydberg gases [1], coherent backscattering of light in cold atoms [2], resonant energy transfer in photosynthetic complexes [3, 4], interatomic Coulombic decay [5, 6], sub- [7] and superradiance [8], and multipartite entanglement [9, 10]. Sensing these interactions in dilute systems of atoms is challenging, especially in presence of significant Doppler shifts introduced by thermal motion.

Manifestations of dipolar interactions in inhomogeneously broadened atomic ensembles can be revealed via so-called *quantum coherence* signals [11–15], which are emitted when atoms are pumped and probed by a series of femtosecond laser pulses (see Fig. 1). Until now, interpretation of such signals [11, 12, 16] has relied on two orthodox premises of multi-dimensional nonlinear spectroscopy [17, 18]: (i) the laser-atom interactions are sufficiently weak and can be accounted for perturbatively, using double-sided Feynman diagrams, and (ii) the dipole-dipole coupling scales as  $\sim R^{-3}$  with the interatomic distance  $R$  and corresponds to the familiar *static* [19], or *near-field* interaction associated with virtual photons [20]. The static interatomic potential gives rise to shifts in the atomic energy levels which are assessed non-perturbatively [11–16] via transformation to the exciton basis [17]. Therefore, in this framework, quantum coherence signals are sensing the exchange of infinitely many *virtual* photons between the atoms.

In this paper, we propose a quantum-optical master equation approach to describe the interaction of dilute thermal gases with ultrashort laser pulses. The same theoretical approach was previously used to faithfully model coherent backscattering (CBS) of intense, continuous wave (cw) laser light by cold atoms [21–24]. By construction, this method treats the laser-matter interaction *non-perturbatively*. Furthermore, the dipole-dipole coupling emerges from an embedding of the atoms into the common electromagnetic bath, upon tracing over its degrees of freedom [25, 26]. In addition to the near-field term, the resulting dipole coupling includes a *far-field* component, which scales as  $\sim R^{-1}$ . This contribution accounts for the retardation of the dipole-dipole interactions and is responsible for *multiple scattering* [24] of *real* photons [20] between atoms. The retarded dipole-dipole

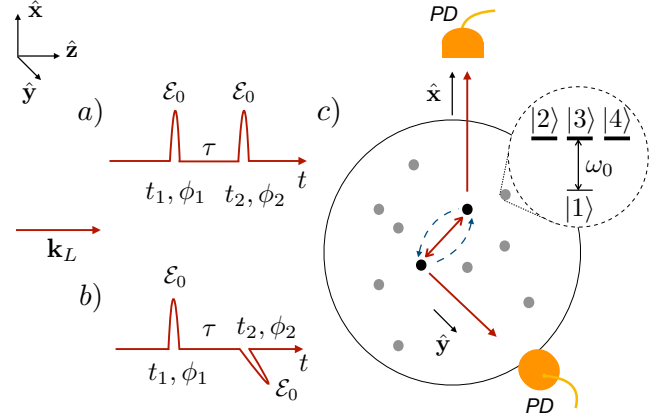


Figure 1. Setup for the observation of multiple quantum coherence (MQC) signals. Two phase-tagged, femtosecond, pump and probe laser pulses with variable time delay  $\tau$  propagate along the  $z$  axis defined by the wave vector  $\mathbf{k}_L$ . The pulses have (a) parallel linear polarizations along the  $x$ -axis; (b) orthogonal linear polarizations along the  $x$ - and  $y$ -axes, respectively. (c) Disordered sample of identical atomic scatterers with electronic dipole transition  $J_g = 0 \rightarrow J_e = 1$  at frequency  $\omega_0$ . The fluorescence signal monitored by the photodetectors (PD) is observed in two directions,  $\hat{\mathbf{x}}$  and/or  $\hat{\mathbf{y}}$ . The red solid arrows indicate real photons exchanged between (emitted by) the atoms, while the dashed blue arrows represent virtual photons.

interaction prevails in dilute gases ( $\sim 10^{10}$  atoms/cm<sup>3</sup>), where the mean interatomic separation is larger than the resonant optical wave length. We can therefore treat this interaction perturbatively and will interpret quantum coherence signals as arising from multiple scattering of single photons between interacting atoms.

Below, we present our formalism and introduce the fluorescence measurement setup (see Fig. 1) that was employed to detect the dipole-dipole interactions in dilute thermal gases [12, 27, 28]. Ultimately, we derive 1QC (single quantum coherence) and 2QC (double quantum coherence) spectra that are in excellent qualitative agreement with recent experiment [28].

*Master equation approach.*— We consider  $N$  identical, initially unexcited, atoms at uncorrelated random positions  $\mathbf{r}_\alpha$  ( $\alpha = 1, \dots, N$ ), immersed into an electro-

magnetic bath represented by an infinite set of quantized harmonic oscillators in their vacuum state. The atoms are driven by pairs of collinear, polarized, femtosecond laser pulses [see Fig. 1(a,b)] with wave vector  $\mathbf{k}_L$  and carrier frequency  $\omega_L$  that is quasi-resonant with the atomic transition frequency  $\omega_0$ . We denote the arrival time of the first (second) pulse in a pair by  $t_1$  ( $t_2$ ), with delay  $\tau = t_2 - t_1$ . After the second pulse, the scattered fluorescence signal is detected in the observation direction  $\hat{\mathbf{k}} \perp \mathbf{k}_L$ , at times  $t_2 \leq t \leq T_{\text{int}}$ , with  $T_{\text{int}}$  an integration time that is much longer than the atomic radiative lifetime.

The signal is expressed through the quantum-mechanical expectation value of the intensity operator, averaged over atomic configurations,

$$I_{\hat{\mathbf{k}}}(t) = \left\langle \left\langle \mathbf{E}_{\hat{\mathbf{k}}}^{(-)}(t) \cdot \mathbf{E}_{\hat{\mathbf{k}}}^{(+)}(t) \right\rangle \right\rangle_{\text{conf}}, \quad (1)$$

where  $\langle \dots \rangle = \text{Tr}[\dots \rho(0)]$ . The initial density operator  $\rho(0)$  of the  $N$ -atom-field system factorises into the ground state of the atoms and the vacuum state of the field. The positive/negative frequency part  $\mathbf{E}_{\hat{\mathbf{k}}}^{(+/-)}(t)$  of the operator for the electric far-field emitted by the atoms in the direction  $\hat{\mathbf{k}}$  reads explicitly [26],

$$\mathbf{E}_{\hat{\mathbf{k}}}^{(+)}(t) = f \sum_{\alpha=1}^N \left\{ \mathbf{D}_{\alpha}(t) - \hat{\mathbf{k}}[\hat{\mathbf{k}} \cdot \mathbf{D}_{\alpha}(t)] \right\} e^{-i\mathbf{k} \cdot \mathbf{r}_{\alpha}}, \quad (2)$$

where  $f = \omega_0^2 d / (4\pi\epsilon_0 c^2 R_d)$ ,  $d$  is the reduced dipole matrix element,  $\epsilon_0$  is the free space permittivity,  $c$  is the speed of light, and  $R_d$  is the distance from the center of mass of the cloud to the detector. In writing Eq. (2), we assume that  $R_d \gg r_{\alpha\beta} = |\mathbf{r}_{\alpha} - \mathbf{r}_{\beta}|$  for any  $\alpha, \beta$ . The atomic lowering (raising) operator  $\mathbf{D}_{\alpha}(t)$  ( $\mathbf{D}_{\alpha}^{\dagger}(t)$ ) for atom  $\alpha$  incorporates arbitrary degeneracies of the ground and excited state sublevels, and  $\mathbf{k}$  is the wave vector of the scattered light. Finally,  $\langle \dots \rangle_{\text{conf}}$  stands for the configuration, or disorder, average. The latter stems from thermal motion of the atoms during the fluorescence detection time, and integrates over interatomic distances, as well as over the orientations of the vectors  $\mathbf{r}_{\alpha\beta}$  connecting pairs of atoms. We denote the mean interatomic distance by  $\bar{r}$  [29], and assume an isotropic distribution of the atoms.

We here specialize to atoms possessing a  $J_g = 0 \rightarrow J_e = 1$  transition, which involves three sublevels in the excited state (see Fig. 1). A crucial consequence of the excited state degeneracy is the existence of levels that are not driven by the laser, but can nevertheless be populated by the dipole-dipole interaction. The atomic lowering operator is given by

$$\mathbf{D}_{\alpha} = -\hat{\mathbf{e}}_{-1}\sigma_{12}^{\alpha} + \hat{\mathbf{e}}_0\sigma_{13}^{\alpha} - \hat{\mathbf{e}}_{+1}\sigma_{14}^{\alpha}, \quad (3)$$

where  $\sigma_{lk}^{\alpha} = |k\rangle_{\alpha}\langle l|_{\alpha}$ , with the excited state sublevels  $|2\rangle, |3\rangle, |4\rangle$  (see Fig. 1) corresponding to magnetic quantum numbers  $-1, 0, +1$ , respectively, and  $\hat{\mathbf{e}}_{\pm 1} = \mp(\hat{\mathbf{x}} \pm$

$i\hat{\mathbf{y}})/\sqrt{2}$ ,  $\hat{\mathbf{e}}_0 = \hat{\mathbf{z}}$ . Using Eqs. (2) and (3), for  $\hat{\mathbf{k}} = \hat{\mathbf{x}}$  in Eq. (1) we obtain

$$I_{\hat{\mathbf{x}}} = \left\langle f^2 \sum_{\alpha, \beta=1}^N e^{ik_0 \hat{\mathbf{x}} \cdot \mathbf{r}_{\alpha\beta}} \left( \langle \sigma_{z1}^{\alpha} \sigma_{1z}^{\beta} \rangle + \langle \sigma_{y1}^{\alpha} \sigma_{1y}^{\beta} \rangle \right) \right\rangle_{\text{conf}}, \quad (4)$$

and  $I_{\hat{\mathbf{y}}}$  follows upon replacing  $\hat{\mathbf{x}} \rightarrow \hat{\mathbf{y}}$ ,  $y \rightarrow x$  in Eq. (4). Note that in the above equation, we dropped the time argument and introduced a new atomic basis,  $|x\rangle = (|4\rangle - |2\rangle)/\sqrt{2}$ ,  $|y\rangle = (|4\rangle + |2\rangle)/(\sqrt{2}i)$ , and  $|z\rangle = |3\rangle$ .

Evaluation of the fluorescence intensity (4) includes that of certain time-dependent atomic dipole correlators. These can be obtained from the Lehmburg-type master equation [25, 26]:

$$\langle \dot{Q} \rangle = \sum_{\alpha=1}^N \langle \mathcal{L}_{\alpha} Q \rangle + \sum_{\alpha \neq \beta=1}^N \langle \mathcal{L}_{\alpha\beta} Q \rangle, \quad (5)$$

where  $Q$  is an arbitrary atomic operator, and the Liouvillians  $\mathcal{L}_{\alpha}$  and  $\mathcal{L}_{\alpha\beta}$  generate the time evolution for independent and interacting atoms, respectively. In the frame rotating at the laser frequency, the Liouvillians read [21, 22, 30]

$$\begin{aligned} \mathcal{L}_{\alpha} Q &= -i\delta [\mathbf{D}_{\alpha}^{\dagger} \cdot \mathbf{D}_{\alpha}, Q] \\ &\quad - \frac{id}{\hbar} [\mathbf{D}_{\alpha}^{\dagger} \cdot \mathbf{E}_L(\mathbf{r}_{\alpha}, t) + \mathbf{D}_{\alpha} \cdot \mathbf{E}_L^*(\mathbf{r}_{\alpha}, t), Q] \\ &\quad + \frac{\gamma}{2} \left( \mathbf{D}_{\alpha}^{\dagger} \cdot [Q, \mathbf{D}_{\alpha}] + [\mathbf{D}_{\alpha}^{\dagger}, Q] \cdot \mathbf{D}_{\alpha} \right), \end{aligned} \quad (6)$$

$$\begin{aligned} \mathcal{L}_{\alpha\beta} Q &= \mathbf{D}_{\alpha}^{\dagger} \cdot \overleftrightarrow{\mathbf{T}}(k_0 r_{\alpha\beta}, \hat{\mathbf{n}}) \cdot [Q, \mathbf{D}_{\beta}] \\ &\quad + [\mathbf{D}_{\beta}^{\dagger}, Q] \cdot \overleftrightarrow{\mathbf{T}}^*(k_0 r_{\alpha\beta}, \hat{\mathbf{n}}) \cdot \mathbf{D}_{\alpha}, \end{aligned} \quad (7)$$

where  $\delta = \omega_L - \omega_0$ ,  $\mathbf{E}_L(\mathbf{r}_{\alpha}, t)$  the slowly varying, complex amplitude of the laser field at the position of atom  $\alpha$ ,  $\gamma$  the spontaneous decay rate, and  $\overleftrightarrow{\mathbf{T}}(k_0 r_{\alpha\beta}, \hat{\mathbf{n}})$  the dipole-dipole interaction tensor, with  $k_0 = \omega_0/c$ , and  $\hat{\mathbf{n}} = \mathbf{r}_{\alpha\beta}/r_{\alpha\beta}$ . Substituting  $\xi = k_0 r_{\alpha\beta}$ , the tensor  $\overleftrightarrow{\mathbf{T}}(\xi, \hat{\mathbf{n}})$  is given by

$$\begin{aligned} \overleftrightarrow{\mathbf{T}}(\xi, \hat{\mathbf{n}}) &= (3\gamma/4)e^{-i\xi} \left[ (i/\xi)(\mathbf{1} - \hat{\mathbf{n}}\hat{\mathbf{n}}) \right. \\ &\quad \left. + (1/\xi^2 - i/\xi^3)(\mathbf{1} - 3\hat{\mathbf{n}}\hat{\mathbf{n}}) \right], \end{aligned} \quad (8)$$

where  $\mathbf{1}$  is a  $3 \times 3$  unit matrix and  $\hat{\mathbf{n}}\hat{\mathbf{n}}$  is a  $3 \times 3$  dyadic. We recall that the far- and near-field terms, scaling respectively as  $\xi^{-1}$  and  $\xi^{-3}$ , are the  $\xi \gg 1$  and  $\xi \ll 1$  asymptotes of the general dipole-dipole interaction tensor (8) [20]. Under the assumption that  $\xi \gg 1$ , which we will henceforth employ, Eq. (8) can be approximated by the far-field term,  $\overleftrightarrow{\mathbf{T}}(\xi, \hat{\mathbf{n}}) \approx (3\gamma/4)g(\xi)(\mathbf{1} - \hat{\mathbf{n}}\hat{\mathbf{n}})$ , responsible for the exchange of transversely polarized (real) photons, with coupling parameter  $g(\xi) = ie^{-i\xi}/\xi$ ,  $|g(\xi)| \ll 1$ .

The dynamics of independent atoms, as generated by the Liouvillians  $\mathcal{L}_{\alpha}$  alone, can be found using known non-perturbative methods [31, 32]. Because of the short duration of the laser-atom interaction (two fs pulses with

delay  $\tau \sim 10$  ps) as compared to the typical thermal coherence time [33] of  $\sim 10$  ns [34], the atoms can be considered at fixed positions for a single interaction event.

The weakness of the dipole-dipole interaction justifies a perturbative solution of Eq. (5) in powers of  $\mathcal{L}_{\alpha\beta}$ . The dynamics thus generated is relevant on timescales exceeding the thermal coherence time, where we cannot ignore atomic motion. Upon averaging over atomic coordinates, all position-dependent phases in  $I_{\mathbf{k}}$  vanish regardless of the observation direction. Thereby, only incoherent terms in Eq. (4) remain, which correspond to the case  $\alpha = \beta$ . Furthermore, we restrict our perturbative expansion to the lowest order in  $\mathcal{L}_{\alpha\beta}$  which survives the disorder average. As a result, each pair of interacting atoms yields a contribution proportional to  $|g(\bar{\xi})|^2 = 1/\bar{\xi}^2$ , where  $\bar{\xi} = k_0\bar{r}$ . Such coupling describes double scattering of a single photon. Finally, only particular products of the matrix elements of  $\vec{\mathbf{T}}(\bar{\xi}, \hat{\mathbf{n}})$  contribute to the average signal upon integration over the isotropic distribution of the vector  $\hat{\mathbf{n}}$  [22, 23]. These non-vanishing combinations can be most compactly expressed in the spherical basis as  $\langle \vec{\mathbf{T}}_{qq'} \vec{\mathbf{T}}_{q'q}^* \rangle_{\text{conf}} = \langle \vec{\mathbf{T}}_{qq'} \vec{\mathbf{T}}_{q'q}^* \rangle_{\text{conf}} \neq 0$  (with  $\vec{\mathbf{T}}_{qq'} = \hat{\mathbf{e}}_q^* \cdot \vec{\mathbf{T}} \cdot \hat{\mathbf{e}}_{q'}$ ,  $q, q' = -1, 0, 1$ ). This imposes restrictions on the atomic sublevels that can be coupled via double (in general, multiple) scattering, in a disordered system.

*Phase-modulated spectroscopy.*— To obtain  $I_{\mathbf{k}}(t)$  from which MQC (multiple quantum coherence) signals can be deduced, we now focus on a sequence of laser pulses that is specific to phase-modulated spectroscopy [35]. Therein, a typical experiment consists of  $M \gg 1$  cycles, each of which lasts for  $T_{\text{int}} \gg \gamma^{-1}$  and involves driving the matter system by two time-delayed, phase-tagged femtosecond pulses, followed by the atomic decay to the ground state [12, 28]. The slowly varying amplitude of the driving field during the interval  $\tau_m \leq t \leq \tau_{m+1}$  ( $0 \leq m \leq M-1$ ) [with the time  $\tau_m = mT_{\text{int}}$  marking the beginning of the  $m$ th pulse] is given by

$$\mathbf{E}_L(\mathbf{r}, t) = \sum_{j=1}^2 \varepsilon_L^{(j)} \mathcal{E}_L(t - t_j^{(m)}) e^{i(\mathbf{k}_L \cdot \mathbf{r} + \Omega_j \tau_m)}, \quad (9)$$

where  $\mathcal{E}_L(t) = \mathcal{E}_0 \exp(-t^2/2\sigma^2)$  is the Gaussian pulse envelope (which we assume to be the same for both pulses), with pulse amplitude  $\mathcal{E}_0$  and duration  $\sigma$ ,  $\varepsilon_L^{(j)}$  is the polarization of the  $j$ th pulse ( $\varepsilon_L^{(1,2)} = \hat{\mathbf{x}}$  or  $\varepsilon_L^{(1)} = \hat{\mathbf{x}}$  and  $\varepsilon_L^{(2)} = \hat{\mathbf{y}}$ ),  $t_j^{(m)}$  the pulse arrival times [36], and the phase tags  $\phi_j =: \Omega_j \tau_m$  ( $j = 1, 2$ ) [see Fig. 1(a,b)] are generated by transmitting the pulses through two acousto-optic modulators oscillating at slightly different frequencies  $\Omega_j$ . In Eq. (9), we used the approximation  $\Omega_j t_j^{(m)} \simeq \Omega_j \tau_m$  [35] and set the initial (constant) phases of the pulses to zero. As a consequence of the phase tagging of the driving field, the signal is modulated at harmonics of the

beat frequency  $\Omega_{21} = \Omega_2 - \Omega_1$ , with the  $\kappa$ th harmonic identifying the  $\kappa$ th quantum coherence ( $\kappa$ QC) [12].

Following the second (probe) pulse, a time-integrated fluorescence signal is monitored in the far field during the time interval  $\tau_{m+1} - t_2^{(m)} \gg \gamma^{-1}$ , and can be approximated by the integral

$$\bar{I}_{\mathbf{k}}(\tau, \tau_m) = \frac{1}{T_{\text{int}}} \int_{t_2^{(m)}}^{\tau_{m+1}} dt I_{\mathbf{k}}(t). \quad (10)$$

Fluorescence signals incident on a photodetector generate a photocurrent that is proportional to  $\bar{I}_{\mathbf{k}}(\tau, \tau_m)$ . The recorded photocurrent is demodulated by multiplication with the reference signal  $e^{-i\kappa\Omega_{21}\tau_m}$  ( $\kappa = 1, 2$  is the demodulation order) [12, 35]. The combined current is filtered by a lock-in narrowband filter described by the kernel  $\Gamma e^{-\Gamma\tau_m}$ , with the lock-in bandwidth  $\Gamma \rightarrow 0$  in the final expression. The demodulated signal is eventually analysed in frequency space, after Fourier-transforming it with respect to the delay  $\tau$ . The above steps can be summarized, in one expression, as [16, 35]

$$S_{\mathbf{k}}(\omega, \kappa) = \lim_{\Gamma \rightarrow 0} \frac{\Gamma}{\sqrt{2\pi}} \int_0^\infty d\tau e^{-i\omega\tau} \int_0^\infty d\tau_m \bar{I}_{\mathbf{k}}(\tau, \tau_m) \times e^{-(\Gamma + i\kappa\Omega_{21})\tau_m}. \quad (11)$$

*Results.*— We now present our results based on a two-atom model – the simplest framework required to deduce 1QC and 2QC signals. Previously, such models proved useful in describing the dipole-dipole interactions in dilute and optically thin atomic ensembles [21, 38].

For  $N = 2$ , the average instantaneous fluorescence intensity can be written as

$$I_{\mathbf{k}}(t) = I_{\mathbf{k}}^{[0]}(t) + I_{\mathbf{k}}^{[2]}(t), \quad (12)$$

where the superscripts indicate powers of  $|g(\bar{\xi})|$ . Since the laser-matter interaction occurs on a time scale much shorter than that induced by the coupling to the electromagnetic bath (which gives rise to the radiative decay of the atoms, and to the dipole-dipole interaction), the Gaussian laser pulses can be modelled by delta pulses carrying the same energy  $E_{\text{pulse}}$ . Such pulses are characterised solely by their pulse area  $\Theta = 2d(\sigma c \mu_0 E_{\text{pulse}} \sqrt{\pi}/A)^{1/2}/\hbar$ , with  $A$  the laser beam's cross-section and  $\mu_0$  the free space permeability.

With this delta-pulse approximation and the ansatz (12), we obtain analytical solutions for  $I_{\mathbf{k}}(t)$ ,  $\bar{I}_{\mathbf{k}}(\tau, \tau_m)$ , and  $S_{\mathbf{k}}(\omega, \kappa)$  [39]. In Fig. 2 we plot the spectra  $S_{\mathbf{k}}(\omega, \kappa)$ , for  $\hat{\mathbf{k}} = \hat{\mathbf{x}}, \hat{\mathbf{y}}$  and  $\kappa = 1, 2$  (1QC and 2QC signals), with the parameter values listed in the caption coinciding with actual experimental ones [28]. We observe that the real and imaginary parts of the 1QC spectra, respectively, exhibit absorptive and dispersive resonances at  $\omega = \omega_0$ , and the 2QC spectra feature qualitatively identical line shapes, albeit with the opposite sign of the 1QC spectra,

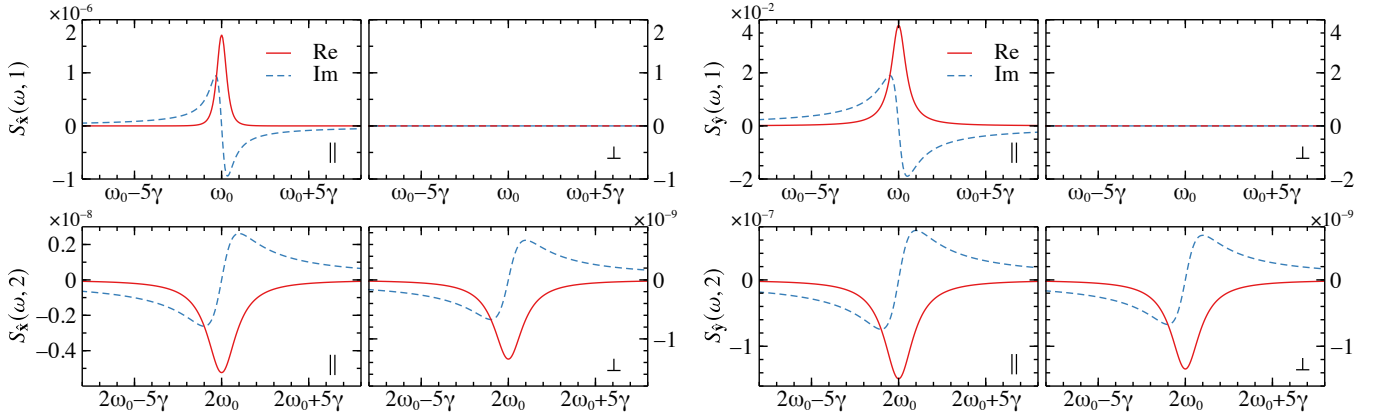


Figure 2. Real (solid lines) and imaginary (dashed lines) parts of the fluorescence spectra  $S_{\hat{\mathbf{k}}}(\omega, \kappa)$  [in units of  $f^2/(T_{\text{int}}\gamma^2)$ ; see Eq. (11)], for  $\hat{\mathbf{k}} = \hat{\mathbf{x}}$  (left block of panels) and  $\hat{\mathbf{k}} = \hat{\mathbf{y}}$  (right block), and for  $\kappa = 1$  (top) and  $\kappa = 2$  (bottom). Symbols  $\parallel$  and  $\perp$  indicate parallel ( $\hat{\mathbf{x}}\text{-}\hat{\mathbf{x}}$ ) and perpendicular ( $\hat{\mathbf{x}}\text{-}\hat{\mathbf{y}}$ ) pump-probe polarizations, respectively. All plots were obtained for particle density  $7 \times 10^{10} \text{ cm}^{-3}$ , corresponding to a mean atomic distance  $\bar{r} \approx 10 \mu\text{m}$ , and for laser pulses with  $E_{\text{pulse}} = 30 \text{ nJ}$ ,  $\delta = 0$ ,  $A = 1 \text{ mm}^2$ ,  $\sigma = 21 \text{ fs}$  [28], tuned in resonance with the D2-line of  $^{87}\text{Rb}$  atoms [37]:  $\gamma \approx 2\pi \times 6.067 \text{ MHz}$ ,  $k_0c = 2\pi \times 384 \text{ THz}$ , and  $d = 4.02ea_0/\sqrt{2}$ , tantamount to a mean value  $\bar{\xi} = k_0\bar{r} \approx 80$ , and to a single pump/probe pulse area  $\Theta = 0.44$ .

at  $\omega = 2\omega_0$ . In the regime of relatively weak (perturbative) laser pulses, the line shapes of the 1QC spectra  $S_{\hat{\mathbf{k}}}(\omega, 1)$  are consistently proportional to the real and imaginary parts of the linear susceptibility [35], while the opposite sign of  $S_{\hat{\mathbf{k}}}(\omega, 2)$  stems from two additional interactions of the atoms with the laser pulses.

Note the complete absence in our data of the 1QC signal in the case of perpendicular ( $\perp$ ) pump-probe polarization (see Fig. 2), corroborating the experiment [28]. This is due to the fact that orthogonally polarized laser pulses imprint the correct phase for demodulation only on Zeeman coherences (off-diagonal atomic density matrix elements in the excited state manifold) – which do not directly lead to fluorescence in the  $\hat{\mathbf{x}}$  or  $\hat{\mathbf{y}}$  directions, see Eq. (4). Zeeman coherences can however be converted to excited state population of the other atom, via the dipole-dipole interaction described by the products  $\overleftrightarrow{\mathbf{T}}_{qq'} \overleftrightarrow{\mathbf{T}}_{q''q}^*$  ( $q' \neq q''$ ), and thus give rise to fluorescence for each configuration. Nevertheless, the net signal vanishes because these products do not survive the disorder average.

In the same pump-probe configuration, 2QC signals are however present. They originate from Zeeman coherences induced in both atoms. Given such a doubly-excited state, the coupling  $\mathcal{L}_{\alpha\beta}$  mediates a collective dissipative process, whereupon a photon is emitted by both atoms. This process is linear in  $\overleftrightarrow{\mathbf{T}}_{qq'}$  (or  $\overleftrightarrow{\mathbf{T}}_{qq'}^*$ ) and, hence, does not contribute to the signal on average. As a result of the photon emission, both atoms are prepared in a coherent superposition of their ground and one of the excited states. Electronic coherence of one atom can be transformed via double scattering into the excited state population of the other atom with a probability proportional to  $\overleftrightarrow{\mathbf{T}}_{qq'}^*$  (or  $\overleftrightarrow{\mathbf{T}}_{qq'}$ ). Since the total proba-

Table I. Peak amplitudes  $\text{Re}\{S_{\hat{\mathbf{k}}}(\omega_0, 1)\}$  and  $\text{Re}\{S_{\hat{\mathbf{k}}}(2\omega_0, 2)\}$  (up to a common prefactor), at leading order in  $\Theta$  and  $1/\bar{\xi}$ , for  $\hat{\mathbf{k}} = \hat{\mathbf{x}}, \hat{\mathbf{y}}$  and for pump-probe polarizations  $\parallel$  and  $\perp$  (see Fig. 2).

$\kappa$	$\hat{\mathbf{k}} = \hat{\mathbf{x}}$		$\hat{\mathbf{k}} = \hat{\mathbf{y}}$	
	$\parallel$	$\perp$	$\parallel$	$\perp$
1	$\frac{3}{10\bar{\xi}^2}\Theta^2$	0	$\Theta^2$	0
2	$-\frac{3}{320\bar{\xi}^2}\Theta^4$	$-\frac{3}{1280\bar{\xi}^2}\Theta^4$	$-\frac{171}{640\bar{\xi}^2}\Theta^4$	$-\frac{3}{1280\bar{\xi}^2}\Theta^4$

bility of preparing such an excited state is proportional to  $\overleftrightarrow{\mathbf{T}}_{qq'} \overleftrightarrow{\mathbf{T}}_{qq'}^*$ , fluorescence from this state *does* give rise to a non-vanishing average signal.

As for the the 1QC signals detected for parallel ( $\parallel$ ) pump-probe polarization ( $\hat{\mathbf{x}}$ , for pump and probe), the peak magnitude for  $\hat{\mathbf{k}} = \hat{\mathbf{x}}$  is four orders of magnitude smaller than for  $\hat{\mathbf{k}} = \hat{\mathbf{y}}$ , see Fig. 2. The reason is that, in the former case, the signal is due to the double scattering contribution  $I_{\hat{\mathbf{x}}}^{[2]}$  alone [see Eqs. (4) and (12)]: Indeed, for parallel polarization of pump and probe, independent atoms cannot emit into the  $\hat{\mathbf{x}}$  direction. In contrast, they can emit in the  $\hat{\mathbf{y}}$  direction, and the single-scattering contribution  $I_{\hat{\mathbf{y}}}^{[0]}$  does not vanish in this circumstance.

Finally, the cause of the different peak values of 1QC and 2QC signals lies in their distinct scaling with the pulse area  $\Theta$ : We find that  $S_{\hat{\mathbf{k}}}(\omega, 1) \propto \Theta^2$ , while  $S_{\hat{\mathbf{k}}}(\omega, 2) \propto \Theta^4$ , see Table I. Different numerical prefactors for different polarization/observation channels stem from the angular integrals. It is notable that, for parallel pump-probe polarization, the ratio  $\text{Re}\{S_{\hat{\mathbf{x}},\parallel}(2\omega_0, 2)\}/\text{Re}\{S_{\hat{\mathbf{x}},\parallel}(\omega_0, 1)\} \propto \Theta^2$  is  $\bar{\xi}$ -

independent (i.e., insensitive to the atomic density), in accord with previous reports [11, 28]. Moreover, we obtain that for both  $\hat{\mathbf{k}} = \hat{\mathbf{x}}, \hat{\mathbf{y}}$ , the ratio  $\text{Re}\{S_{\hat{\mathbf{k}},\parallel}(2\omega_0, 2)\}/\text{Re}\{S_{\hat{\mathbf{k}},\perp}(2\omega_0, 2)\}$  depends neither on  $\bar{\xi}$  nor on  $\Theta$  – a prediction that is yet to be confirmed experimentally.

*Conclusions.* — We have described multiple quantum coherence (MQC) signals in dilute, thermal atomic vapors. The distinctive feature of our method is the non-perturbative (perturbative) treatment of the laser-matter (dipole-dipole) interactions, implemented in a master equation approach that fully accounts for the exchange of virtual and real photons. In this perspective, MQC signals are sensing the *retarded* dipole-dipole interactions mediated by the *exchange of real photons*. While, in our present work, we obtained single and double quantum coherence signals, our method defines a general and versatile framework for the systematic assessment of higher-order contributions – which were observed experimentally [12, 27, 28] – by combining diagrammatic expansions in the far-field dipole-dipole coupling with single-atom responses to laser pulses of arbitrary strength [23, 24]. In the future, we will explore the non-perturbative regime of the laser-atom interactions and study how strong external driving can be used to enhance specific signals [32]. Finally, we will generalize our method to resolve more subtle features of MQC spectra [27] – due to fine and hyperfine structures of the involved dipole transitions.

The authors wish to thank Robert Bennett, Lukas Bruder, Daniel Finkelstein-Shapiro, and Frank Stienkemeier for useful and enjoyable discussions. E. G. C. acknowledges the support of the G. H. Endress Foundation. V. S. and A. B. thank the Strategiefonds der Albert-Ludwigs-Universität Freiburg for partial funding.

- 
- [1] M. D. Lukin, M. Fleischhauer, R. Cote, L. M. Duan, D. Jaksch, J. I. Cirac, and P. Zoller, *Phys. Rev. Lett.* **87**, 037901 (2001).
- [2] G. Labeyrie, F. de Tomasi, J.-C. Bernard, C. A. Müller, C. Miniatura, and R. Kaiser, *Phys. Rev. Lett.* **83**, 5266 (1999).
- [3] T. Brixner, J. Stenger, H. M. Vaswani, M. Cho, R. E. Blankenship, and G. R. Fleming, *Nature (London)* **434**, 625 (2005).
- [4] V. N. Shatokhin, M. Walschaers, F. Schlawin, and A. Buchleitner, *New J. Phys.* **20**, 113040 (2018).
- [5] L. S. Cederbaum, J. Zobeley, and F. Tarantelli, *Phys. Rev. Lett.* **79**, 4778 (1997).
- [6] J. L. Hemmerich, R. Bennett, and S. Y. Buhmann, *Nature Commun.* **9**, 2934 (2018).
- [7] T. Bienaimé, N. Piovella, and R. Kaiser, *Phys. Rev. Lett.* **108**, 123602 (2012).
- [8] S. J. Roof, K. J. Kemp, M. D. Havey, and I. M. Sokolov, *Phys. Rev. Lett.* **117**, 073003 (2016).
- [9] F. Platzer, F. Mintert, and A. Buchleitner, *Phys. Rev. Lett.* **105**, 020501 (2010).
- [10] S. Sauer, F. Mintert, C. Gneiting, and A. Buchleitner, *J. Phys. B* **45**, 154011 (2012).
- [11] X. Dai, M. Richter, H. Li, A. D. Bristow, C. Falvo, S. Mukamel, and S. T. Cundiff, *Phys. Rev. Lett.* **108**, 193201 (2012).
- [12] L. Bruder, M. Binz, and F. Stienkemeier, *Phys. Rev. A* **92**, 053412 (2015).
- [13] F. Gao, S. T. Cundiff, and H. Li, *Opt. Lett.* **41**, 2954 (2016).
- [14] B. Lomsadze and S. T. Cundiff, *Phys. Rev. Lett.* **120**, 233401 (2018).
- [15] S. Yu, M. Titze, Y. Zhu, X. Liu, and H. Li, *Opt. Express* **27**, 28891 (2019).
- [16] Z.-Z. Li, L. Bruder, F. Stienkemeier, and A. Eisfeld, *Phys. Rev. A* **95**, 052509 (2017).
- [17] S. Mukamel, *Principles of Nonlinear Optical Spectroscopy* (Oxford University Press, New York, 1995).
- [18] J. A. Leegwater and S. Mukamel, *Phys. Rev. A* **49**, 146 (1994).
- [19] J. D. Jackson, *Classical Electrodynamics*, 3rd ed. (Wiley, New York, 1998).
- [20] D. L. Andrews and D. S. Bradshaw, *Eur. J. Phys.* **25**, 845 (2004).
- [21] V. Shatokhin, C. A. Müller, and A. Buchleitner, *Phys. Rev. Lett.* **94**, 043603 (2005).
- [22] V. Shatokhin, C. A. Müller, and A. Buchleitner, *Phys. Rev. A* **73**, 063813 (2006).
- [23] A. Ketterer, A. Buchleitner, and V. N. Shatokhin, *Phys. Rev. A* **90**, 053839 (2014).
- [24] T. Binninger, V. N. Shatokhin, A. Buchleitner, and T. Wellens, *Phys. Rev. A* **100**, 033816 (2019).
- [25] R. H. Lehmann, *Phys. Rev. A* **2**, 883 (1970).
- [26] G. S. Agarwal, *Quantum Statistical Theories of Spontaneous Emission and their Relation to other Approaches* (Springer, Berlin, 1974).
- [27] L. Bruder, “*Nonlinear phase-modulated spectroscopy of doped helium droplet beams and dilute gases*,” Dissertation (Albert-Ludwigs-Universität Freiburg, 2017).
- [28] L. Bruder, A. Eisfeld, U. Bangert, M. Binz, M. Jakob, D. Uhl, M. Schulz-Weiling, E. R. Grant, and F. Stienkemeier, *Phys. Chem. Chem. Phys.* **21**, 2276 (2019).
- [29] For a particle density  $n$ ,  $\bar{r} \simeq 0.554n^{-1/3}$  [18].
- [30] J. Guo and J. Cooper, *Phys. Rev. A* **51**, 3128 (1995).
- [31] L. Allen and J. Eberly, *Optical Resonance and Two-Level Atoms* (Dover Publications, Inc., New York, 1987).
- [32] L. Chen, E. Palacino-González, M. F. Gelin, and W. Domcke, *J. Chem. Phys.* **147**, 234104 (2017).
- [33] G. Labeyrie, D. Delande, R. Kaiser, and C. Miniatura, *Phys. Rev. Lett.* **97**, 013004 (2006).
- [34] The thermal coherence time  $\lambda/v \approx 10$  ns can be obtained from the Doppler shift  $k_0 v \approx 560$  MHz and the wavelength  $\lambda = 2\pi/k_0 \approx 790$  nm [28].
- [35] P. F. Tekavec, T. R. Dyke, and A. H. Marcus, *J. Chem. Phys.* **125**, 194303 (2006).
- [36] Although  $t_j^{(m)}$  and  $\phi_j$  depend on  $m$ , to not overburden the notation, we drop the label  $m$  in Fig. 1.
- [37] D. A. Steck, “*Rubidium 87 D Line Data*,” .
- [38] T. Jonckheere, C. A. Müller, R. Kaiser, C. Miniatura, and D. Delande, *Phys. Rev. Lett.* **85**, 4269 (2000).
- [39] B. Ames, “*Dynamical detection of dipole-dipole interactions in dilute atomic gases*,” Master Thesis (Albert-Ludwigs-Universität Freiburg, 2019).